

# Color representations of normals and congenital red–green color deficiencies: Estimation of individual results based on color vision model

Minoru Ohkoba<sup>1</sup>  | Tomoharu Ishikawa<sup>2</sup> | Shoko Hira<sup>3</sup> | Sakuichi Ohtsuka<sup>4</sup> | Miyoshi Ayama<sup>5</sup> 

<sup>1</sup>Graduate School of Engineering, Utsunomiya University, Japan

<sup>2</sup>School of Engineering, Utsunomiya University, Japan

<sup>3</sup>Graduate School of Science and Engineering, Kagoshima University, Japan

<sup>4</sup>Department of Science and Technology, International College of Technology, Kanazawa, Japan

<sup>5</sup>Center for Optical Research and Education, Utsunomiya University, Japan

## Correspondence

Minoru Ohkoba, Graduate School of Engineering, Utsunomiya University, Japan.

Email: dt187102@cc.utsunomiya-u.ac.jp

## Funding information

Japan Society for the Promotion of Science, Grant/Award Number: 15K00278

## Abstract

Difference scaling experiment was conducted to investigate the mental color representation of congenital color-deficient observers and observers with normal color vision. Two decks of cards, high and medium chroma, each containing 10 Munsell chips, were prepared. A total of 45 pairs of hues were prepared for each of the decks. Ten protans, 10 deutans, and 10 people with normal color vision participated as observers, with each asked to rate the perceptual distance between two colors on a given color card. The results were analyzed using the multidimensional scaling method. All observers with normal color vision showed a circular shape close to the Munsell hue circle, while the majority of color-deficient observers showed a concave shape bending at Y and PB. To indicate the degree of distortion from a circle, the distortion index was proposed to quantitatively evaluate intergroup and individual differences. To investigate the underlying mechanism of intergroup differences as well as individual differences in color representations of observers with normal color vision and color-deficient observers, we proposed a model that considers various levels of human color vision mechanism from the cone pigment absorption, the luminance and opponent-color coding level, and nonlinear transformation to difference-scaling judgment. The circular shape for observers with normal color vision and some color-deficient observers, as well as concave shapes for most color-deficient observers were estimated. The correlation coefficient between the estimation and experiment-based difference ranged from  $r = 0.64$  to  $r = 0.94$  with the grand average of  $r = 0.82$ , with  $p$ -values less than 0.001 for all observers, suggesting that the concept of proposed model is appropriate.

## KEY WORDS

congenital color vision deficiency, deutan, hue circle, MDS, protan

This is an open access article under the terms of the Creative Commons Attribution-NonCommercial-NoDerivs License, which permits use and distribution in any medium, provided the original work is properly cited, the use is non-commercial and no modifications or adaptations are made.

© 2021 The Authors. Color Research and Application published by Wiley Periodicals LLC.

## 1 | INTRODUCTION

### 1.1 | Background and Aim of the study

The S, M, and L cones, each, respectively, sensitive to short, middle, and long-wavelength regions of the visible spectrum, are the three types of photoreceptors in the retina that determine normal human color vision. Congenital red-green color vision deficiency is caused by the lack of M or L cones (dichromat) or the wavelength shift in M- or L-cone sensitivity (anomalous trichromat). In this study, these color-deficient observers are referred to as "CDOs", and the observers with normal color vision, as "CNOs." Other types of congenital color vision deficiencies such as tritanopia, caused by a lack of S-cone function, cone monochromacy, associated with the function of only one type of cone, and rod monochromacy, which is caused by the lack of all types of cones, are not considered in this study. Among CDOs, dichromats are classified into two types: protanopes (individuals who lack the L cone function) and deutanopes (those lack the M cone function). Similarly, anomalous trichromats are classified into two types: protanomalous, those with M and M-like cones, and deuteranomalous, those with L and L-like cones, sensitive to the middle to long-wavelength lights, respectively.<sup>1,2</sup> Deuteranomaly is the most common type of anomalous trichromacy with a wide range of severity of color vision deficiency and is considered to be linked with the spectral separation between the two L cone pigments.<sup>3</sup> In this study, protan and deutan refer protanopic and protanomalous observers, and deuteranopic and deuteranomalous observers, respectively.

CDOs have difficulty in discriminating some combinations of color, which are easily discriminable for CNOs, for example, pale orange and light green, or gray and magenta of the same degree of lightness. Consequently, enormous number of comparative studies have been conducted CDOs' color discrimination as compared with that of CNOs to investigate the properties of color vision mechanisms, develop effective color vision tests, and provide a database for universal color design.<sup>4-9</sup>

In contrast to the accumulated knowledge on color discrimination, only a few studies have reported on the difference in color representation between CDOs and CNOs. Color representation here refers to the manner in which hues, brightness, and saturation are arranged in the observer's mental color representation. Shepard and Cooper<sup>10</sup> tackled this issue and discovered contrasting differences in the color representations of CDOs and CNOs based on a "similarity scaling" experiment using pairs of color stimuli. They drew multidimensional scaling (MDS) configurations that reflect how the color stimuli are arranged in the observer's mental representation based on visual perception for the observers of various

types of color vision, including CNOs and CDOs. The MDS configuration of CNOs was represented by a circular shape similar to the hue circle in ordinal color order systems such as the Munsell color system. However, the MDS configuration of CDOs displayed a concave shape bending at yellow and turquoise. The distance between red and green was much closer than that of CNOs, reflecting the low level of discriminability between the two colors. Subsequently, several studies have reported perceptual color representations of CDOs and CNOs showing MDS configurations based on different experiments.<sup>11-14</sup> However, their main focus was to investigate the differences among different types of color vision. Thus, only the representative MDS results of each group were indicated. Few studies have reported on the differences in color representation in individual CDOs.

As previously mentioned, the severity of red-green color deficiency covers a wide range from weak anomalous trichromats to strong dichromats. Ordinal color vision tests reveal the degree of severity for individual observers; however, they do not disclose the individual properties of internal color representation. Determining how vision-based colors are arranged in an individual mental representation is useful for various aspects, such as ascertaining the color combinations that are poorly discriminable for an individual, or customizing color reproduction in a personal display. Recently, color customization has received attention because of the widespread use of personal devices.<sup>15,16</sup> Vision-based color representation for individual observers is essential and useful for optimizing the color reproduction of a new device for personal use. For example, perceived difference between typical red and green, or typical orange and light green differs among individual CDOs. Thus, to enhance color differences between typical color pairs to compensate the individual perceived similarity between some color pairs by preparing customized 3D-Look-up-table would be possible if we have vision-based color representation data, instead of assumed color enhancement according to the type of color deficiency now available in web or mobile application.

Therefore, we aimed to investigate the common property of vision-based color representation of CNOs and two types of CDOs and to reveal the range of individual variability. We further proposed a model to explain individual differences using pre-existing visual mechanisms.

### 1.2 | Previous studies

Shepard and Cooper<sup>10</sup> reported their results based on their long-term research on the representation of colors in persons with different visual sensory systems. They employed 14 CNOs, 11 CDOs of protan and deutan,

1 monochromat, 6 observers with total blindness, and 5 other miscellaneous weaker color anomalies, whose data were not included in the article. First, they selected nine color names of "red," "orange," "gold," "yellow," "green," "turquoise," "blue," "violet," and "purple." Three kinds of card decks for sighted observers were prepared: 1) printed color names, 2) color chip pairs that correspond to the above color names, and 3) color chip pairs with color names. In addition, a card deck on which color names were written by raised braille characters was prepared for blind observers. Each deck was composed of 36 cards and pair combinations of nine colors or color names. All cards were shuffled and presented to the observer who was asked to rearrange the cards according to their similarity ranking. The experimental results were analyzed by various methods, but the most closely related to this study is the MDS configurations of CNOs, CDOs, and monochromat for Names Only and Color Only conditions shown in Figure 2 in their study. The MDS configuration of Names Only for CNOs and CDOs both became more or less circular in the hue order of ordinal color order systems such as the Munsell color system. However, while this represented interesting findings, our primary focus was on the results of the color cards. The MDS configuration of Colors Only for CNOs showed a circular shape similar to that of Names only, while the configuration for CDOs and the monochromat became concave. In addition, the bending positions of the CDOs were very clear at yellow and turquoise. They showed the range of individual variability in the weight space of the blue-yellow versus red-green plane and the first and second dimensions of the MDS, respectively, but did not show how and to what degree the MDS configuration varied among observers of each color vision type.

Paramei<sup>11</sup> conducted an elementary color-naming experiment for three CNOs, one protanope, and one deuteranomalous observer using 17 monochromatic stimuli to reconstruct their color space. Observers were allowed to use a maximum of three color names from a selection of "red," "yellow," "green," "blue," and "white" to express the color perception of a given stimulus. A total of 10 points were assigned according to the number of color names used, and the responses were treated as five-dimensional vectors to input into the MDS analysis. Results were expressed in three-dimensional space with red-green, blue-yellow, and saturation axes. The CNO's arrangement of 17 stimuli was presented along a continuous curve in 3D space in the wavelength order, whereas CDOs showed a cluster of middle wavelength stimuli in the second quadrant out of wavelength order. In their study, however, number of observers was one for each of CDO types.

Paramei et al.<sup>14</sup> showed group MDS configurations based on "color-dissimilarity" judgment for five CNOs,

two protans, and four deutans, separately. They also constructed a "group color space" based on all observers, and individual property was expressed by compression or elongation along its axes and the angle of rotation on the plane of the first and second dimensions. Parameters to express individual property were elaborately plotted on the polar diagram; however, how and to what extent the MDS configurations of individual CNOs and CDOs varied was not indicated.

Bonnardel<sup>12</sup> indicated color category maps of the combined data of 39 CNOs and individual data of 5 deutans based on free sorting, constrained sorting, and constrained-naming tasks using 140 Munsell chips of 20 basic hues with seven lightness values for each at the highest chroma available. The similarity between the two chips was then calculated from the degree of consensus among observers for all pairs to perform the MDS analysis. They employed a unique method of converting color categorization data to psychological distance in which the distance between two different chips is zero when each observer chooses the same category for both, while it is maximum when all observers choose different categories for each of them. The MDS results were plotted in a 3D space. The first and second dimensions corresponded to the green-[pink/purple] and blue-[yellow/orange] axes, were labeled as G-R and B-Y, respectively. The third axis for CNO was associated with lightness, whereas the comprehension of CDOs was not clearly identifiable. Individual color category maps of 140 Munsell chips for five deutan observers are presented in Figure 1 in their study; however, the perceptual color spaces, that is, the MDS configurations, were representative of each color vision type because they were derived from individual variability within each group.

Lillo et al.<sup>13</sup> also carried out categorical color mapping and best example selection experiments using 11 basic color terms for 15 CNOs, 8 protanopes, and 9 deuteranopes against 102 color chips. Similarity between two chips was derived by the methods essentially similar to Bonnardel's study, to construct "confusion" matrix for all pairs of the chips to perform the MDS analysis. The color representation of CNOs was expressed well by the 3D model in which three axes related to the red-green, yellow-blue, and lightness, were consistent with previous results,<sup>11,12</sup> whereas for that of CDOs, both protans and deutans were properly indicated in the 2D model in which the first and second axes seem to be chromatic of blue versus orange and achromatic of white versus black, respectively. In this study, only the representative color space of each group was indicated for the same reason as in Bonnardel's study.

Each of the previous studies cited above had their own objective and showed valuable results pertinent to

their purpose. However, they did not indicate the MDS configuration, that is, the internal color space of multiple individuals of each color vision type and thus did not discuss about the cause of individual differences either. We consider that it would be valuable to show individual

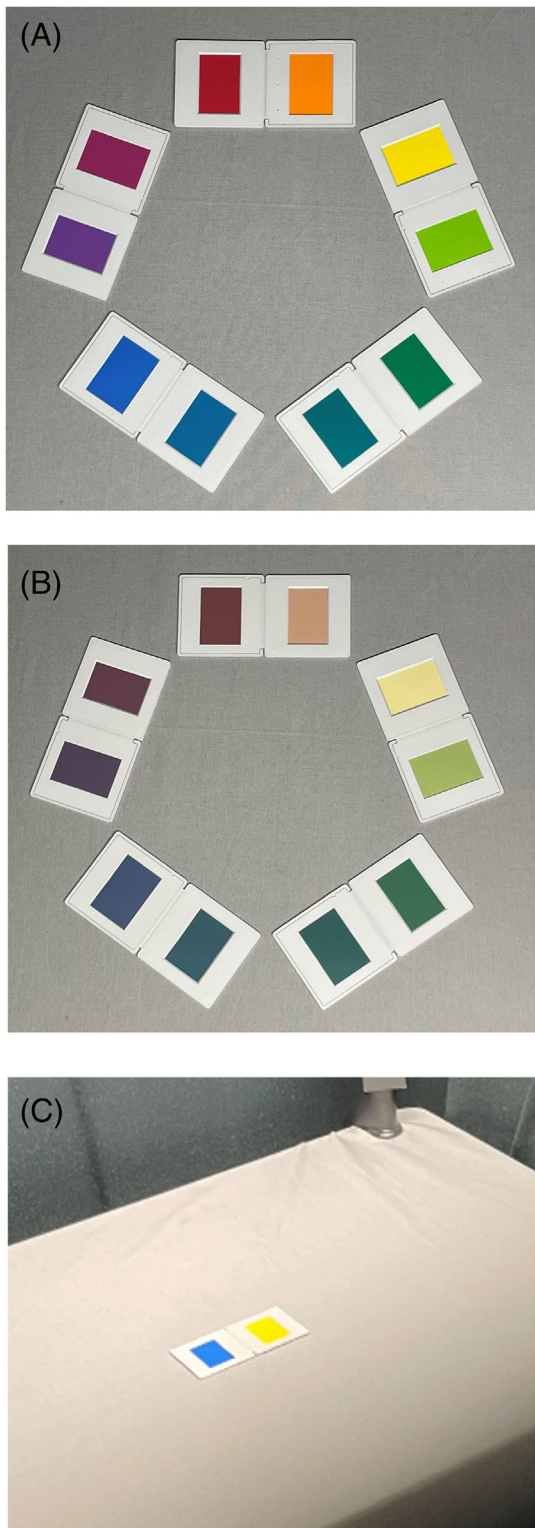


**FIGURE 1** Examples of color cards of high chroma chips (A), medium chroma chips (B), and the card on the table in the experiment (C)

internal color space for CNOs and both types of CDOs, because to explore individual variability gives us a hint of difference in underlying mechanism to determine the judgment. This study intends to present the internal color space of multiple observers from different color vision types and their variability range and to propose a model to explain individual differences in difference scaling of colors.

## 2 | EXPERIMENT

In this study, the judgment is referred to as “difference scaling” instead of “similarity scaling” because the perceptual difference of all pairs employed was suprathreshold, even for CDOs, and thus the two chips appeared more or less different. This is merely a naming issue; however, its usage is exactly the same as “similarity scaling” in Shepard and Cooper.<sup>10</sup>

### 2.1 | Stimuli

Two decks of stimuli, high and medium chroma, were prepared. Each consisted of Munsell color chips of five primary and five secondary hues with different lightness values. The Munsell notation is shown in Table 1. High chroma chips were chosen as the same stimuli employed in the study by Okudera et al.,<sup>17</sup> who compared the color space of CNOs and blind observers. High chroma R, YR, Y, G, PB, and P are very close to the focal colors of red, orange, yellow, green, blue, and purple, respectively, as reported by Sturges and Whitfield,<sup>18</sup> which indicates that they are similarly close to the focal colors of Berlin and Kay.<sup>19</sup> B is situated on the greenish border of their blue region, GY is found on the interior of the green region but near the yellowish border, BG is between the blue and green regions, and RP is between the purple

**TABLE 1** Munsell notation of the color chips and the labels

Labels	High chroma	Medium chroma
R	5R 4/14	5R 4/4
YR	5YR 6.5/14	5YR 6.5/4
Y	5Y 8/14	5Y 8/4
GY	5GY 6.5/10	5GY 6.5/4
G	5G 4.5/10	5G 4.5/4
BG	5BG 4/9	5BG 4/3
B	5B 4/8	5B 4/3
PB	5PB 4/12	5PB 4/4
P	5P 4/11	5P 4/3
RP	5RP 4/12	5RP 4/4

and pink regions. Medium chroma chips were chosen from the same hue as the high chroma group; however, the Munsell chroma was either 3 or 4. All combinations of 10 hues (i.e., 45 pairs) were prepared for each of the high and medium chroma groups. Two color chips were put in the enclosure consisted of two opened 35 mm slide mounts, which are referred to hereafter as “color card.” The size of the color area was 25 mm × 35 mm, and the edges of the chips were 25 mm apart. The slide mount was achromatic and appeared close to the gray scale of N8. Figure 1A,B shows five examples of color cards of high and medium chroma chips, respectively, and Figure 1C the card on the table in the experiment.

## 2.2 | Observation environment

A desk 75 cm wide and 50 cm deep, covered by a gray cloth (close to N6.5), was placed in a darkroom. A color card was placed near the center of the desk surface and was illuminated by a fluorescent light (CCT: 5000 K), as shown in Figure 1C. Spectral irradiance at the center of the desk illuminated by the fluorescent lamp measured by the illuminance spectrophotometer (CL-500A; Konica Minolta, Inc.) is indicated in Figure 2. The horizontal illuminance at the color card was 560 lx, and the irradiance was 1.72 W/m<sup>2</sup>. The visual distance in the observation was approximately 50 cm.

## 2.3 | Procedure

At the beginning of the experiment, the aim of the study and the content of the experiments were explained by the experimenter outside the darkroom. Informed consent forms developed according to the Utsunomiya University code of ethics for research were signed by each observer. Subsequently, each observer was asked to enter the dark room. The experiment began 10 min after observer's

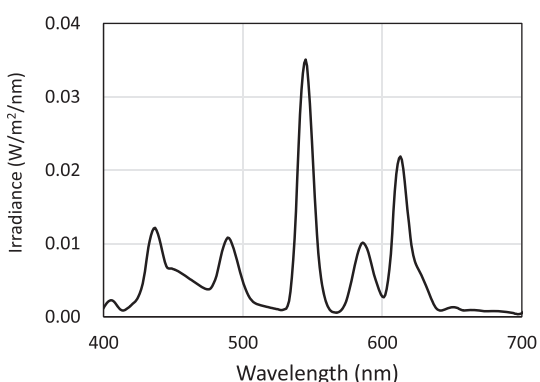


FIGURE 2 Spectral irradiance measured at the center of the desk illuminated by the fluorescent lamp

adaptation to the light in the visual environment. The experimenter then placed a color card in front of the observer and asked the observer to rate the perceptual distance between the two colors on a given color card using a scale of 1 (very close), 2 (rather close), 3 (neither close nor far), 4 (rather far), and 5 (very far). The observer wrote a rating score on the answer sheet that had been given in advance. After the observer wrote their answer, the experimenter took the color card away and provided the next color card. Forty-five color cards were presented in a random order in the first half, subsequent to which a 5–10 min rest period was taken. Following this, the same pairs of 45 color cards were presented in a different random order after inverting the left and right. The experimenter stayed in a small space next to the observing booth separated by a black curtain and entered the booth only to serve a color card. For the high and medium color cards, the same procedure was employed, and at least a 1 h break was taken between the sessions.

In addition to the color card experiments, we performed a similar difference-scaling experiment using written color-name pairs without showing any color cards to observers. However, this study concerns the results of color cards that have sufficient volume. Some color-name results have been reported elsewhere.<sup>20,21</sup>

## 2.4 | Observers

Ten protans (five protanomalous trichromats and five protanopes), 10 deutans (two deuteronomalous trichromats, eight deutanopes), and 10 CNOs participated in the experiment using high chroma color cards. Similarly, nine protans (four protanomalous trichromats and five protanopes), seven deutans (two deuteronomalous trichromats and five deutanopes), and nine CNOs participated in the experiment using medium chroma color cards. The age of the observers ranged from 20 to 46 years, average and the standard deviation are 28.4 and 8.6 years, respectively, with more than 90% of the observers in each color vision type being in their 20s or 30s. All observers were examined for their color vision using Ishihara charts, Panel D-15, and an anomaloscope. The observers were all male Japanese, and either university students or experimental collaborators who were introduced from the Color Universal Design Organization (CUDO). In this study, color vision type was determined based on the results of the anomaloscope because it is considered to be the most accurate test to specify the type and severity of congenital red-green color deficiency.<sup>22</sup> Ishihara charts and Panel D-15 were carried out as subsidiary test to confirm the type of color deficiency. No observers performed a genetic test to identify their visual pigment information. Thus, color vision type might change if their visual pigment genes are

analyzed. Color vision type employed in this study, age, participation to the experiments, and the results of color vision tests of observers are indicated in Table 2. Cross

mark in the matching range of anomaloscope indicates that the stable result was obtained in the two measurements with an interval period of at least half a year.

TABLE 2 Observers' age, color vision type, and their results of color vision tests

Obs.	Age	Color vision type	Anomaloscope	Panel D-15	Ishihara chart
			Matching range	Crossings parallel to protan line	% correct as an ideal normal trichromat
N10	22	N	30–50	0 (pass)	96%
N11	22	N	40	0 (pass)	100%
N12	24	N	40–50	0 (pass)	100%
N13	25	N	40	0 (pass)	100%
N14 <sup>a</sup>	22	N	40	0 (pass)	96%
N15	21	N	40–50	0 (pass)	100%
N16	23	N	40	0 (pass) <sup>b</sup>	100%
N17	23	N	40	0 (pass)	100%
N20	22	N	40	0 (pass)	100%
N32	46	N	40	0 (pass)	100%
Obs.	Age	Color vision type	Anomaloscope	Panel D-15	Ishihara chart
			Matching range	Crossings parallel to protan line	% correct as an ideal protanope
P3	38	PA	10–70 <sup>c</sup>	4.5	76%
P4	30	PA	0–70 <sup>c</sup>	4	64%
P7	21	PA	0–70 <sup>c</sup>	0 (pass)	74%
P8 <sup>a</sup>	23	PA	0–60 <sup>c</sup>	0 (pass)	32%
P9	23	PA	0–70 <sup>c</sup>	4.5	52%
P5	39	P	0–73 <sup>c</sup>	2.5	52%
P10	44	P	0–73 <sup>c</sup>	4	80%
P11	37	P	0–73 <sup>c</sup>	4.5	64%
P14	21	P	0–73	5	76%
P15	39	P	0–73	4.5	60%
Obs.	Age	Color vision type	Anomaloscope	Panel D-15	Ishihara chart
			Matching range	Crossings parallel to deutan line	% correct as an ideal deuteranope
D10	24	DA	0–50 <sup>c</sup>	0 (pass)	82%
D12	22	DA	0–60	6	62%
D7 <sup>a</sup>	34	D	0–73	5	68%
D8	24	D	0–73 <sup>c</sup>	6	76%
D9	24	D	0–73	1	48%
D11	21	D	0–73	5.5	60%
D13 <sup>a</sup>	20	D	0–73 <sup>c</sup>	0 (pass)	74%
D14 <sup>a</sup>	31	D	0–73	4	70%
D17	46	D	0–73	6	64%
D18	40	D	0–73	6	64%

<sup>a</sup>Did not participate the medium chroma experiment.

<sup>b</sup>Two transpositions between cap 3 and cap 8.

<sup>c</sup>Results with repetition.

[Correction added on 28 March 2022, after first online publication. The name of the item in the block at the bottom of Table 2 "Crossings parallel to protan line" has been changed to "Crossings parallel to deutan line" on page 6.]

### 3 | RESULTS

#### 3.1 | Result of the MDS

The average value of the rating scores in the two repetitions was calculated for each of the 45 pairs for each observer for each of the high and medium chroma conditions that were input to the MDS analysis. We employed the iso MDS Kruskal's nonmetric MDS method and applied two, three, and four dimensions to the MDS analysis to determine the optimal number of dimensions. All

MDS analysis was conducted with the statistics software R 3.5.3. "Stress" indicates the degree of discrepancy between the experimental and MDS results.<sup>23</sup> In the cases of 10%, 5%, and 2%, the goodness of fit is fair, good, and excellent, respectively. It was observed that the stress value decreased with an increase in dimension in a similar way among the CNOs, protans, and deutans. Considering that the average stress values of the three groups amounted to less than 5%, we employed the results of a three-dimensional analysis, which were employed in most previous studies.

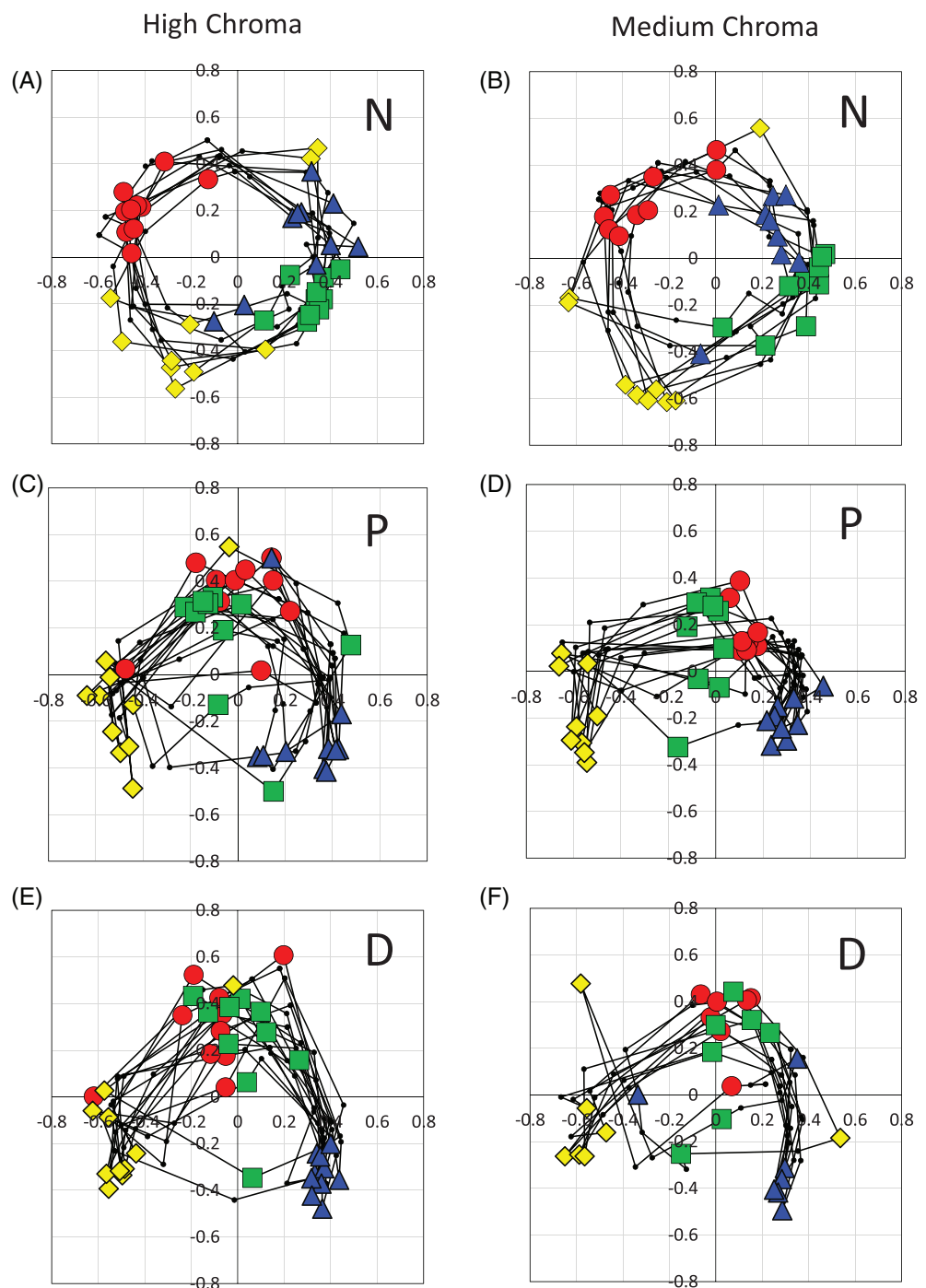


**FIGURE 3** Multidimensional scaling (MDS) configurations of all observers obtained from the high chroma (Figure 3A,C,E in the left column) and medium chroma (Figure 3B,D,F in the right column) card experiments for CNO, protan, deutan observers from top to bottom

Figure 3 shows the results of three-dimensional MDS for all the CNOs, protans, and deutans, plotting the first and second dimension on the  $x$  and  $y$  axes. As shown in the figure, points of the same test stimulus roughly cluster on the  $x$ - $y$  plane indicating common property among observers as described below. In contrast to that, no clear tendency was found along the third dimension with a large individual variation in the results of all color vision types. Causes of the variation are unknown at the present and remain an issue to be solved. Thus, the plots along the third axis are not shown here. In the MDS configuration, points are arranged such that the distances for all pairs are as close to the difference scaling data as possible, thus, a line-symmetric transformation is allowed. To avoid unnecessary confusion, we set the color chip R to be on the positive side of the second (vertical) axis. No transformation was performed on the first (horizontal) axis. To plot the MDS configuration of different observers together, individual MDS was normalized by setting the maximum distance to the same value in Figure 3. The positions of the color chips of R, G, Y, and PB are indicated in the plots by red circles, green squares, yellow diamonds, and blue triangles, respectively.

The figures in the left column (Figure 3A,C,E) and in the right column (Figure 3B,D,F) are the respective results of the high and medium chromas, projected onto the first and second dimensions. The CNOs plot for the high and medium chromas shown in Figure 3A,B are all circular, and the general tendency is very similar. The first axis seems to correlate with the red-green opponency for both high and medium chromas for most observers. Exceptions are the two observers in the high chroma, whose Rs are closer to the vertical axis, and the other two observers in the medium chroma whose Rs are on the vertical axis. The second axis of the high chroma seems to correlate with the yellow-blue opponency; however, the points of Y and PB scatter in a wide area, indicating that it is not a simple yellow-blue opponency but is probably combined with a lightness difference because Y and PB have a fairly large difference in Munsell values. The test stimuli along the third axis were arranged neither according to the lightness order nor the saturation order in all groups, which rendered the comprehension of the axis implication difficult.

Results of protans and deutans shown in Figure 3C,D, E,F, respectively, show similar tendencies as follows: 1) for both the high and medium chroma stimuli, results of most observers show concaved shape bending at Y and PB, referred to as "C-shape" by Shepard and Cooper<sup>10</sup>; 2) Y and PB distribute in the negative and positive sides along the first axis, respectively; 3) for most observers, R and G gather near the vertical axis; 4) for both protans

and deutans, a few observers show circular configuration similar to that of CNOs; 5) for both protan and deutan observers, individual difference seems to be smaller in the medium chroma results as compared to the high chroma results; and 6) for protan observers, degree of concavity becomes smaller in the medium chroma results as compared to the high chroma results. From 2) and 3), the first axis of the majority of the CDOs seems to denote the yellow/blue opponency, and the second axis seems to reflect some chromatic strength that is neither yellowish nor bluish.

### 3.2 | Analysis with distortion index

Figure 3 indicates large individual differences for all groups. To express the shape property of an individual observer's MDS configuration, we introduced an index called *the distortion index (DI)* defined by the following equation:

$$DI = \frac{\pi \cdot d_{\max}^2}{4 \cdot S} \quad (1)$$

where  $S$  and  $d_{\max}$  are the area enclosed by lines that connect the 10 color positions and the farthest distance between the color points, respectively.  $DI$  is equal to 1 when the MDS configuration is circular and increases as the MDS configuration distorts from a circular shape.  $DI$  is the inverse of ASTM (American Society for Testing and Materials) nodularity proposed to evaluate the circularity of particles in materials.<sup>24</sup> The  $DI$  values of all observers are indicated in Table 3. Medium chroma data are missing for some observers because the experiment was done in the last, and those observers were not available at the time because of graduation or inability of scheduling.

Figure 4 shows two examples of individual MDS configurations for high chroma cards from each of the CNO, protan, and deutan groups, as well as those derived from the average data of difference scaling for each group. Observers N10 and N16, shown in Figure 4A,B, respectively, show the minimum and maximum  $DI$  among the 10 CNOs. As shown in the figure, the MDS shape of N10 is almost circular and the sequence of the test stimuli is in the order of Munsell hue circle, whereas that of N16 has some local irregularity. Other observers' MDS configurations were between those of N10 and N16, basically circular but with one or two small dents in most cases. The MDS configuration based on the average data of the difference scaling shown in Figure 4C depicts a circular shape, and 10 chips are arranged more uniformly than individual results. Figure 4D-F shows the results of

TABLE 3 Individual value of *DI*

CNO			CDO (protans)			CDO (deutans)		
Obs. No.	High chroma	Medium chroma	Obs. No.	High chroma	Medium chroma	Obs. No.	High chroma	Medium chroma
N 10	1.25	1.22	P3	7.36	6.82	D 7	6.44	-
N 11	1.57	1.60	P4	4.90	11.50	D 8	11.27	11.24
N 12	1.66	1.46	P5	5.87	11.65	D 9	3.34	14.92
N 13	1.46	1.42	P7	1.97	1.95	D 10	1.34	1.76
N 14	1.82	-	P8	1.39	-	D 11	2.89	11.45
N 15	1.31	1.28	P9	3.47	11.23	D 12	14.69	9.30
N 16	2.05	1.54	P10	3.96	12.45	D 13	1.64	-
N 17	1.35	1.73	P11	15.44	5.66	D 14	10.57	-
N 20	1.36	1.52	P14	5.92	5.33	D 17	4.96	9.73
N 32	1.41	1.24	P15	9.47	9.47	D 18	9.93	9.92

Note: Hyphens indicate the measurement was not done for those observers.

Abbreviations: CNO, normal color vision; CDO, color-deficient observers.

The colors of Obs. in the table are protanopes for dark orange, protanomalous trichromats for pale orange, deuternopes for dark green, and deuteronomalous trichromats for pale green.

protans. The *DI* of P8 in Figure 4D is 1.39, which is the smallest among the protans, shows a circular shape similar to that of the CNOs. The result of P15 in Figure 4E shows a typical concave shape often found in CDOs. His *DI* is 9.47, which is fairly large compared with that of P8 and CNOs, and the second largest among protans. The results based on the average data in Figure 4F show a concave shape reflecting the property indicated by most protan observers. The result of D10 in Figure 4G, where *DI* = 1.34, is the smallest among deutans and is also roughly circular. The result of D18 in Figure 4H shows a concave shape similar to that of P15, for which the *DI* is 9.93. The results based on the average deutan data in Figure 4I show a concave shape, indicating that most observers showed this property similar to the protan group. Based on the data of our 30 observers, the *DI* of the cases that showed partial concavity was approximately 2, and of the cases that showed clear concavity was approximately larger than 5.

Some CDOs show *DI* values comparable to those of CNOs. For example, P8 in high chroma, P7 and D10 in high and medium chroma, and D13 in high chroma. It is interesting that these observers showed no error in Panel D-15 test (See Table 2). However, their matching ranges in the anomaloscope test are definitely wider than normal range indicating their color deficiency. In Panel D-15 test, changes of S-cone and rod excitation among caps are the key factor to correctly arrange the caps.<sup>25</sup> So, these CDOs who perfectly passed D-15 might have S-cone and/or rod channel that works more efficiently to determine color differences than other CDOs. On the other

hand, relatively large value of *DI* of N16 is mainly caused by his tendency in difference scaling. He assigned 5 to the pairs of R versus G, R versus GB, R versus B, and R versus PB while 4, 3.5 and 4 to the pairs of Y versus B, Y versus PB, and Y versus P, resulting ellipsoidal MDS configuration elongated along the R-G axis which made his *DI* largest among CNOs. It is worth noting however, that he is the only one CNO in this study who showed two transpositions, although not parallel to protan, deutan, or tritan lines, in Panel D-15 test.

The values of individual *DI*s are plotted separately in different color vision types for the high and medium chroma card experiments in Figure 5. As shown in the figure, CNOs' results are concentrated in a narrow area around 1.5, whereas the CDO results are distributed over a wider range for both high and medium chromas. We conducted a mixed ANOVA by employing color vision type as between-subjects factor and high and medium chroma as within-subjects factor. Data of observers who participated both high and medium chroma conditions were used to examine within-subjects factor, and data of DA (deuteronomalous) were omitted because there were only two observers. The analysis revealed a main effect of color vision type ( $F(3,19) = 32.2, p < 0.001, \eta^2_G = 0.644$ ) and a main effect of high and medium chroma ( $F(1, 19) = 5.79, p < 0.05, \eta^2_G = 0.164$ ), whereas an interaction between color vision type and chroma ( $F(3,19) = 1.70, p = 0.201, \eta^2_G = 0.147$ ) was lower significance level. Adjusted *p*-values by Bonferroni correction between CNO versus P (protanopes), CNO versus D (deuternopes), and CNO versus PA (protanomalous)

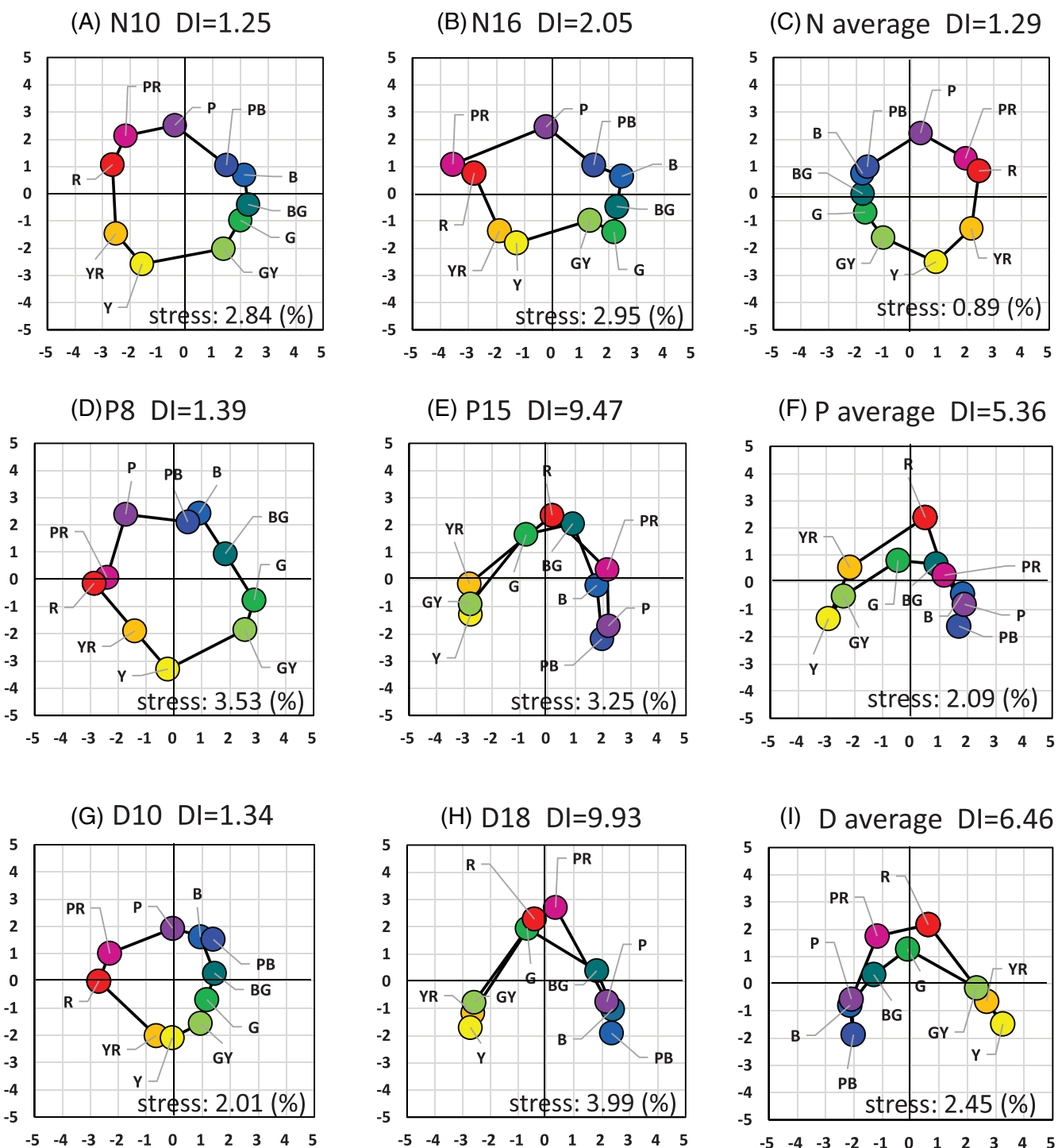


**FIGURE 4** Multidimensional scaling (MDS) configurations obtained from two observers' in the left and center column and average data in the right column of normal (Figure 4A,B,C), protan (Figure 4D,E,F), and deutan groups (Figure 4G,H,I), in the upper, middle, and lower rows, respectively, in the high chroma card experiment

were all less than 0.001, indicating that *DI* of each CDO group is significantly higher than that of CNO's. Further investigation of color vision type effect within high and medium chroma was conducted using planned contrast. It revealed that CNO versus P, D, and PA were ( $t = 4.11$ ,  $p < 0.01$ ), ( $t = 3.49$ ,  $p < 0.05$ ), and ( $t = 1.43$ ,  $p = 0.996$ ) in

the high chroma condition and ( $t = 5.28$ ,  $p < 0.001$ ), ( $t = 7.08$ ,  $p < 0.001$ ), and ( $t = 4.23$ ,  $p < 0.01$ ) in the medium chroma condition, respectively. This indicates that the differences in CNOs versus each of CDO groups are significant in the medium chroma condition, as well as *DI* of PA is not significantly higher than that of CNO

**FIGURE 5** Distortion indices for all observers

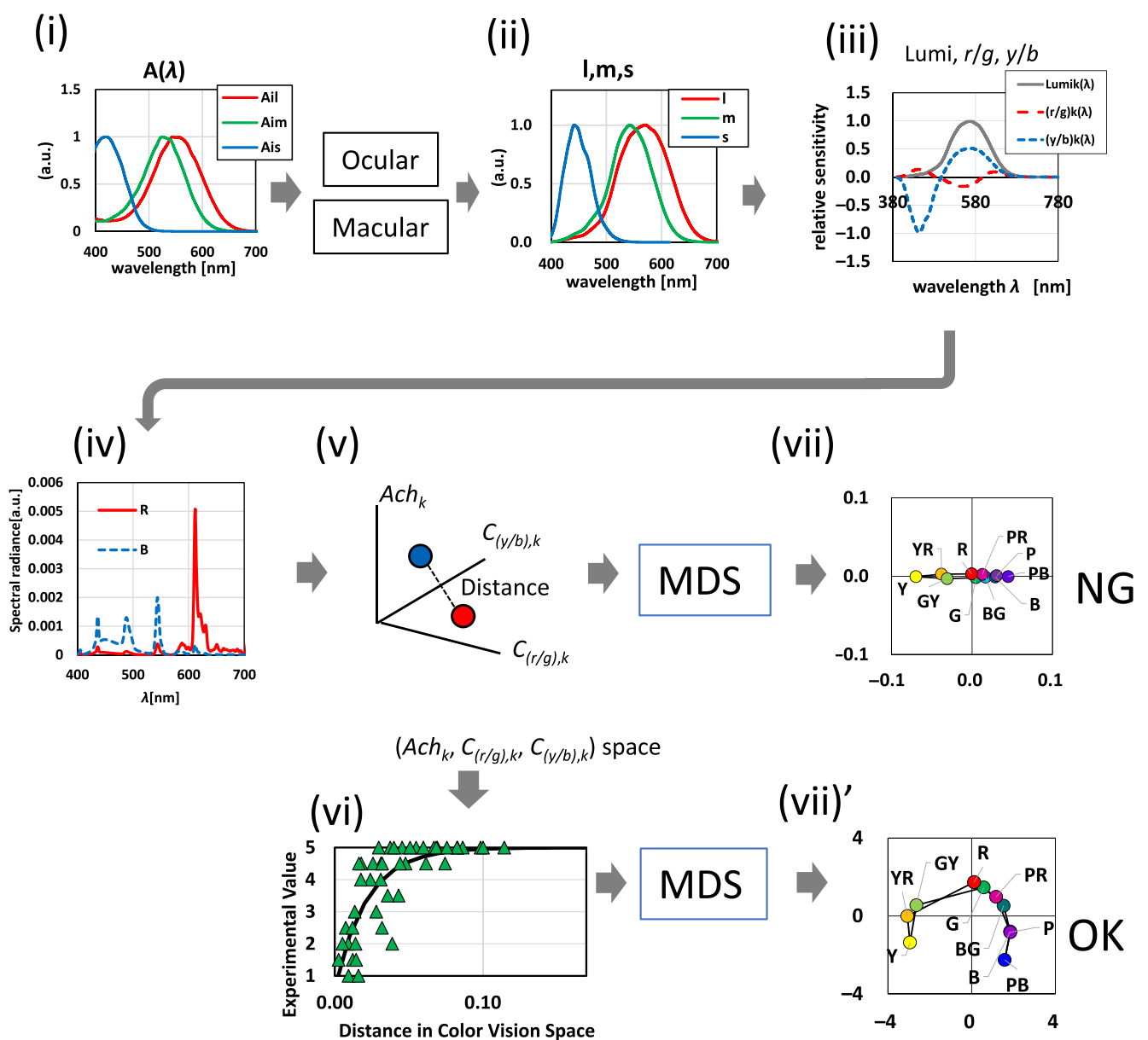
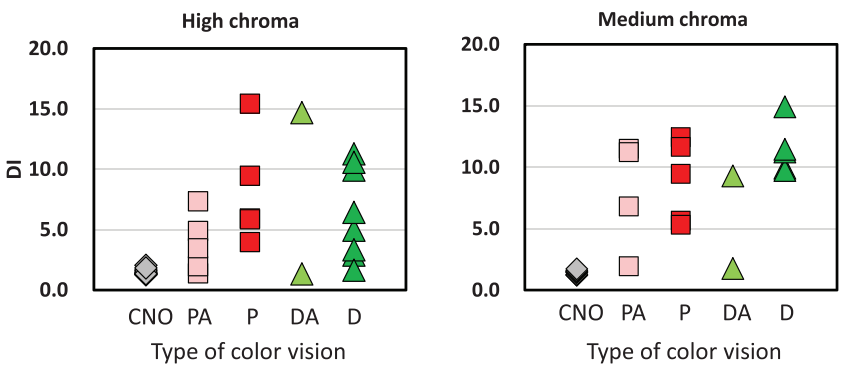


**FIGURE 6** Flow of the simulation process. (i) Spectral absorbance. (ii) Spectral sensitivity. (iii) Spectral sensitivity. (iv) Spectral radiance from the surface of color chip. (v) Distance in  $(Ach_k, C_{(r/g),k}, C_{(y/g),k})$  space. (vi) Assuming a saturation function. (vii)' Result of conventional simulation. (vii)' Result of new simulation

in the high chroma condition, indicating the effect of chroma on the construction of mental color representation.

## 4 | ESTIMATION OF INDIVIDUAL COLOR REPRESENTATION

Our results correlate strongly with the results of CNOs and CDOs in Shepard and Cooper<sup>10</sup> that show color representation of CNOs became similar to hue circle, whereas that of CDOs, of both protans and deutans, shows a C-shape bending at Y and PB (Turquoise in Shepard and Cooper), with R and G placed very closely together. Such a correlation, despite occurring more than two decades apart, with differences in observers' ethnicity, and/or differences in the stimuli and procedure, implies that the color representations of CNOs and CDOs are not affected by cultural factors, but are rather based on the sensory and perceptual system of color inherent in human observers.

In this section, we attempt to estimate individual color representations of CNOs and CDOs from the spectral characteristics of LMS cones in the retina, succeeding processes in color vision mechanisms, and finally to the difference scaling. Such a simulation, first reported in this study, would help us to understand the potential factors explaining the individual differences found in our results.

The flow of the simulation is shown in Figure 6. Steps (i) to (vii) are described as follows:

- i. Absorption spectra of LMS cone pigments (quantum base).
- ii. Conversion to spectral sensitivities of LMS cones (energy base).
- iii. Derivation of luminance (L) and two chromatically opponent processes (r/g and y/b) based on linear transformations of LMS cone spectral sensitivities.
- iv. Obtaining the spectral radiant distribution from the surface of color chips, and computation of the coordinates from that and spectral sensitivity functions of L, r/g, and y/b channels.
- v. Plotting of the color chip coordinates in the color vision space ( $Ach_k$ ,  $C_{(r/g),k}$ ,  $C_{(y/b),k}$ ), and the calculation of distances for all pairs.
- vi. Assumption of a saturation function from the distances to difference scaling.
- (vii)/(vii)' MDS analysis without the step (vi) or with the step (vi).

Calculations of each step will be described in detail in the following sections.

### 4.1 | Cone spectral sensitivities

Yaguchi et al.<sup>26</sup> reported a color appearance simulation for CNOs and CDOs with different degrees of severity. We employed their method in our calculations from (i) to (iii), which is essentially the same as those reported in the technical report of the CIE on the physiological-based color space.<sup>27,28</sup> It is well known that the spectral absorption spectrum of visual pigments shows almost the same curve when plotted along the wave number (called nomogram), and huge variations among visual pigments can be expressed by the shift of the peak.<sup>29</sup> In the simulation, we estimated the cone spectral sensitivity of CDOs from the peak wavelength shift of the pigment absorption spectrum along the wave number axis, which was assumed to be inversely proportional to the distance between the R and G plots relative to  $d_{max}$  in the color representation of each observer, with a maximum shift of  $694\text{ cm}^{-1}$  in that the spectral absorbance of L and M cone pigments overlap. Thus, if R and G overlap with zero distance, the observer is assumed to have only one cone pigment in the middle to long wavelength region. On the other hand, if the distance between R and G is not zero, the observer is assumed to have two cone pigments in that wavelength region, whatever his color vision type determined by the anomaloscope test is. This assumption is qualitatively consistent with the study by Neitz et al.,<sup>3</sup> who reported the relation between color discriminability and spectral separation of pigments. Developments in molecular genetics of visual pigments in these three decades revealed that protanomaly has M- and M-like pigments, and deutanomaly has L- and L-like pigments in the middle to long wavelength region.<sup>1,2</sup> However, to derive the peak shift of the absorption spectrum, we employed the classical concept employed by Yaguchi et al.,<sup>26</sup> where the protanomaly has a normal M-pigment and L'-pigment with a peak shifted from the normal L-pigment toward shorter wavelengths, and deutanomaly has L-pigment and M'-pigment with a peak shifted from the normal M-pigment toward longer wavelengths, for simplicity of calculation. The absolute value of the peak shift in the wave number for observer  $k$ ,  $|\Delta\nu_k|$ , was estimated using the following equation:

$$|\Delta\nu_k| = 694 \cdot \left(1 - \frac{d_{RG,k}}{d_{max,k}}\right) \quad (2)$$

where  $d_{RG,k}$  is the distance between R and G, and  $d_{max,k}$  is the maximum distance in the MDS configuration of the observer  $k$ . As mentioned above, if  $d_{RG,k} = 0$ , then  $|\Delta\nu_k|$  becomes 694, which brings the L'- or M'-pigment perfectly overlaps with the M- or L-pigment, respectively.

None of the observers showed perfect overlap in this study.

In the case of CNO, we derived individual L- and M-pigment absorbances instead of employing the same normal L- and M-pigments, because individual differences in the MDS configuration are non-negligible. We assumed the shift of the L and M cone pigments together with the same amount using Equations (3) and (4). This assumption does not seem inappropriate because the polymorphism that causes wavelength shift of maximum absorption spectrum was found for both of L- and M-pigments of CNOs,<sup>30–32</sup> as well as variability of substructure of L- and M-pigment genes of Japanese male CNOs.<sup>33</sup>

After the amount of shift value along the wave number axis for L- and/or M-pigments was estimated, the spectral absorbance curves of three cone pigments for observer  $k$ , were determined as follows:

$$\log A_{L,k}(\nu) = \log A_L(\nu - |\Delta\nu_k|) \quad (3)$$

$$\log A_{M,k}(\nu) = \log A_M(\nu + |\Delta\nu_k|) \quad (4)$$

$$\log A_{S,k}(\nu) = \log A_S(\nu) \quad (5)$$

In the calculation, we employed the peak wave numbers of normal L, M, and S pigments as  $17\ 538\text{ cm}^{-1}$ ,  $18\ 423\text{ cm}^{-1}$ , and  $22\ 619\text{ cm}^{-1}$ , respectively, with the basic template function of CIE170-1.<sup>27</sup> They were then converted to spectral sensitivity curves in energy units along the wavelength, taking the absorptions of macular pigment and the ocular media into consideration in the same way as in previous studies.<sup>26,27</sup> All spectral sensitivity curves were then normalized at the peak wavelength, denoted as  $l_k(\lambda)$ ,  $m_k(\lambda)$ , and  $s_k(\lambda)$ , which appear in later equations. Peak wavelengths of the spectral sensitivity of the cones with normal L, M, and S pigments mentioned above are 570.2 nm, 542.8 nm, and 442.1 nm, respectively.

## 4.2 | Distances of the color chips in the luminance, r/g, and y/b space

The next step is to calculate the outputs of luminance, red/green, and yellow/blue channels denoted as  $Lumi$ ,  $r/g$ , and  $y/b$ , respectively, for 10 color chips. We employed linear transformations of the cone spectral sensitivities to express the spectral luminous sensitivity and the response functions of opponent-color channels as shown in the following equations:

$$\begin{aligned} Lumi_k(\lambda) &= 0.6899 \left( \frac{L_{EEW}}{L_{EEW,k}} \right) \cdot l_k(\lambda) \\ &\quad + 0.3483 \left( \frac{M_{EEW}}{M_{EEW,k}} \right) \cdot m_k(\lambda) \end{aligned} \quad (6)$$

$$\begin{aligned} (r/g)_k(\lambda) &= 0.8388 \left( \frac{L_{EEW}}{L_{EEW,k}} \right) \cdot l_k(\lambda) \\ &\quad - 1.1191 \left( \frac{M_{EEW}}{M_{EEW,k}} \right) \cdot m_k(\lambda) + 0.1514 \cdot S_k(\lambda) \end{aligned} \quad (7)$$

$$\begin{aligned} (y/b)_k(\lambda) &= 0.3566 \left( \frac{L_{EEW}}{L_{EEW,k}} \right) \cdot l_k(\lambda) \\ &\quad + 0.1800 \left( \frac{M_{EEW}}{M_{EEW,k}} \right) \cdot m_k(\lambda) - S_k(\lambda) \end{aligned} \quad (8)$$

Equation (6) is the  $2^\circ$  spectral luminous efficiency function recommended in the CIE170-2.<sup>28</sup> Equations (7) and (8) are basically the same as those used in Yaguchi et al.'s study.<sup>26</sup> The only difference is adding S-cone contribution to  $(r/g)$  which was necessary to obtain a good fit in the later stage. Coefficients in Equations (7) and (8) are employed so as to make outputs of both  $(r/g)$  and  $(y/b)$  become zero, that is, achromatic for equal energy white and to obtain approximately the same absolute values of integral values of red, green, yellow, and blue portions.

In the above equations, the subscript EEW represents equal energy white. Terms of  $L_{EEW}$  and  $M_{EEW}$  are the stimulus values of equal-energy white for the standard normal trichromats who has the LMS cones with peak sensitivity wavelengths of 570.2 nm, 542.8 nm, and 442.1 nm, respectively. The terms  $L_{EEW,k}$  and  $M_{EEW,k}$  are those for observer  $k$  that are introduced to normalize the equations under the concept that equal-energy white should look white for any observer regardless of the color vision type. The variables  $l_k(\lambda)$ ,  $m_k(\lambda)$ , and  $s_k(\lambda)$  are the spectral sensitivities of the L, M, and S cones of observer  $k$ , respectively, as explained in Section 4.1.

The typical spectral sensitivities of  $Lumi$  and the spectral response functions of the  $r/g$  and  $y/b$  are shown in the upper right graph in Figure 6. Those of representative observers in the three color vision types are indicated in the left column of Figure 7. As shown in Figure 7A, the amplitude of the spectral response function of  $r/g$  is smaller than that of  $y/b$  for observer N10, and thus,  $w_{r/g} = 4.40$  in Equation (10), was needed to fit the experimental data. The same was true for other CNOs, showing that  $w_{r/g}$  ranged from 3.01 to 6.47 with an average of 4.33. Compared with the results of N10, amplitude of  $r/g$  of P15 and D18 shown

in Figure 7C,E, respectively, is smaller, and  $w_{r/g} = 1.05$  and 0.55, respectively, reflecting weaker response of red/green channel. Average values and the ranges of  $w_{r/g}$  for protans and deutans are 1.51, 0.55–3.22, and 0.84, 0–3.36, respectively.

Then, the spectral radiant curve from the surface of each color chip measured under the experimental lighting environment was multiplied by the above spectral functions for each wavelength, summed up across the visible spectrum, and multiplied by appropriate weights to derive the outputs of the three channels of the color chip as shown in the following equations:

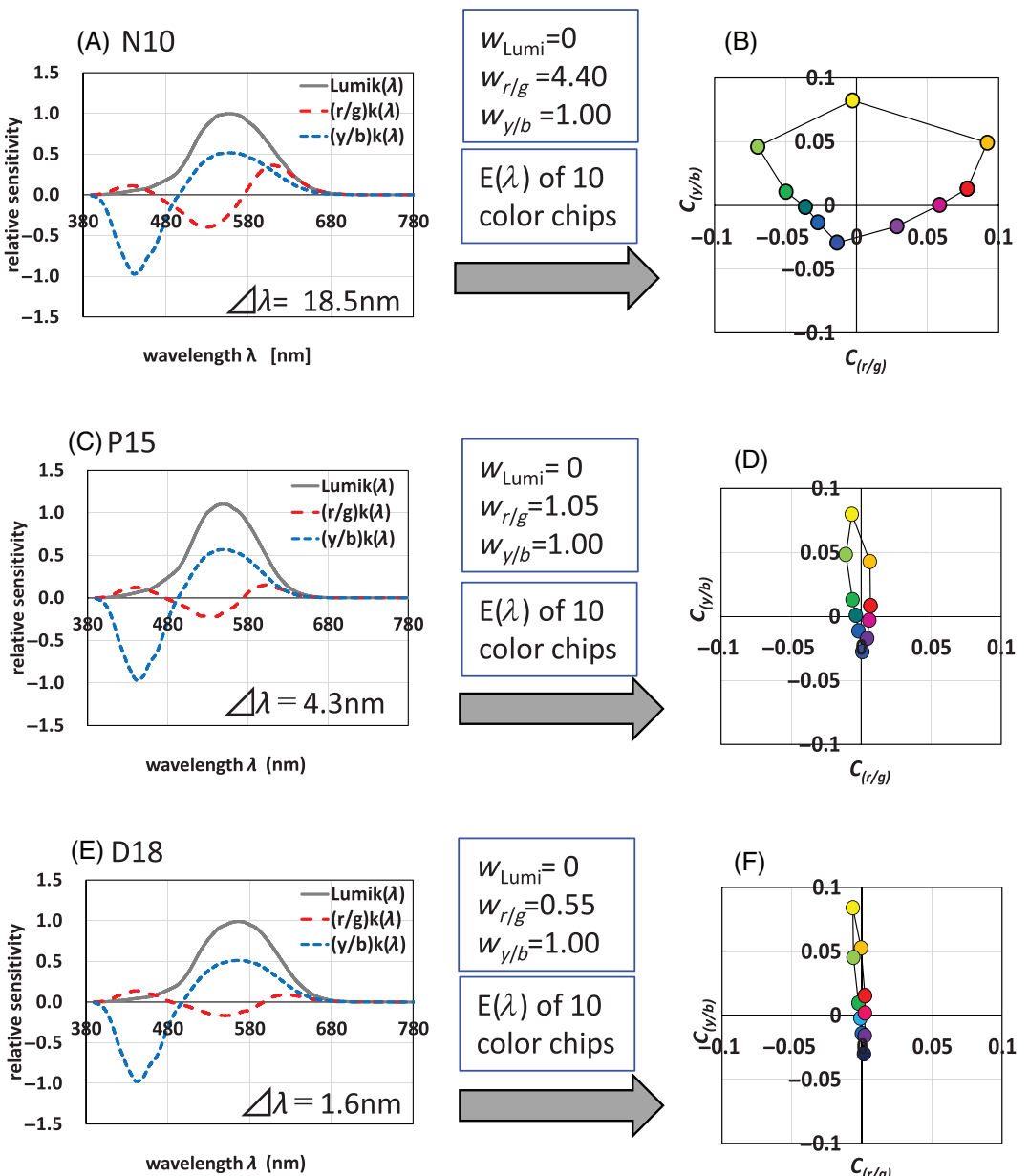


FIGURE 7 Spectral sensitivities of the Lumi, r/g, and y/b channels (A,C, and E on the left), and the positions of 10 color chips in the  $C_{(r/g)}$  versus  $C_{(y/b)}$  plane (B,D, and F on the right) for CNO, protan, and deutan observers from top to bottom

$$Ach_{k,i} = w_{\text{Lumi},k} \cdot \int \text{Lumi}_k(\lambda) \cdot E_i(\lambda) d\lambda \quad (9)$$

$$C_{(r/g),k,i} = w_{(r/g),k} \cdot \int (r/g)_k(\lambda) \cdot E_i(\lambda) d\lambda \quad (10)$$

$$C_{(y/b),k,i} = w_{(y/b),k} \cdot \int (y/b)_k(\lambda) \cdot E_i(\lambda) d\lambda \quad (11)$$

where  $w_{\text{Lumi},k}$ ,  $w_{(r/g),k}$ , and  $w_{(y/b),k}$  are the weighting coefficients for luminance, r/g, and y/b channels for observer  $k$ , respectively. In this study, we fixed the value

$w_{(y/b),k} = 1$ , for the following reasons: First, we started from the setting of  $w_{\text{Lumi},k} = 1$ , but the best fitting was obtained with  $w_{\text{Lumi},k} = 0$  for all observers in the high chroma condition. In addition, the contribution of the  $y/b$  channel to difference scaling was less variant than that of  $r/g$  among different observers. Thus, assuming  $w_{(y/b),k} = 1$  yields relatively comprehensive results. In Equations (9)–(11),  $E_i(\lambda)$  denotes the spectral radiant distribution from the surface of color chip  $i$  in

$(r/g),k$ , and  $w_{(y/b),k}$  positions of 10 color chips on the  $(C_{(r/g)},k)$ ,  $C_{(y/b),k}$ ) planes are indicated in the figures in the right column of Figure 7. Ten chips were placed in the same order as the Munsell hue circle for all observers, but the layouts of CDOs become thinner along the vertical  $C_{(y/b),k}$  axis.

Then, the distance between two different color chips,  $i$  and  $j$  ( $i, j = 1, 2, \dots, 10$ , but  $i \neq j$ ), for observer  $k$ ,  $D_{k,ij}$  was calculated as follows:

$$D_{k,ij} = \sqrt{(Ach_{k,i} - Ach_{k,j})^2 + (C_{(r/g),k,i} - C_{(r/g),k,j})^2 + (C_{(y/b),k,i} - C_{(y/b),k,j})^2} \quad (12)$$

the experimental environment. Note that  $Ach_k$ ,  $C_{(r/g),k}$ , and  $C_{(y/b),k}$  are the outputs of three channels with individual weighting coefficients. In Figure 7,  $w_{\text{Lumi},k}$ ,  $w_{(r/g),k}$ ,

First, we input the distances  $D_{k,ij}$  obtained for 45 pairs directly to the MDS analysis; however, the MDS configuration for CDOs did not show a concave shape, but only

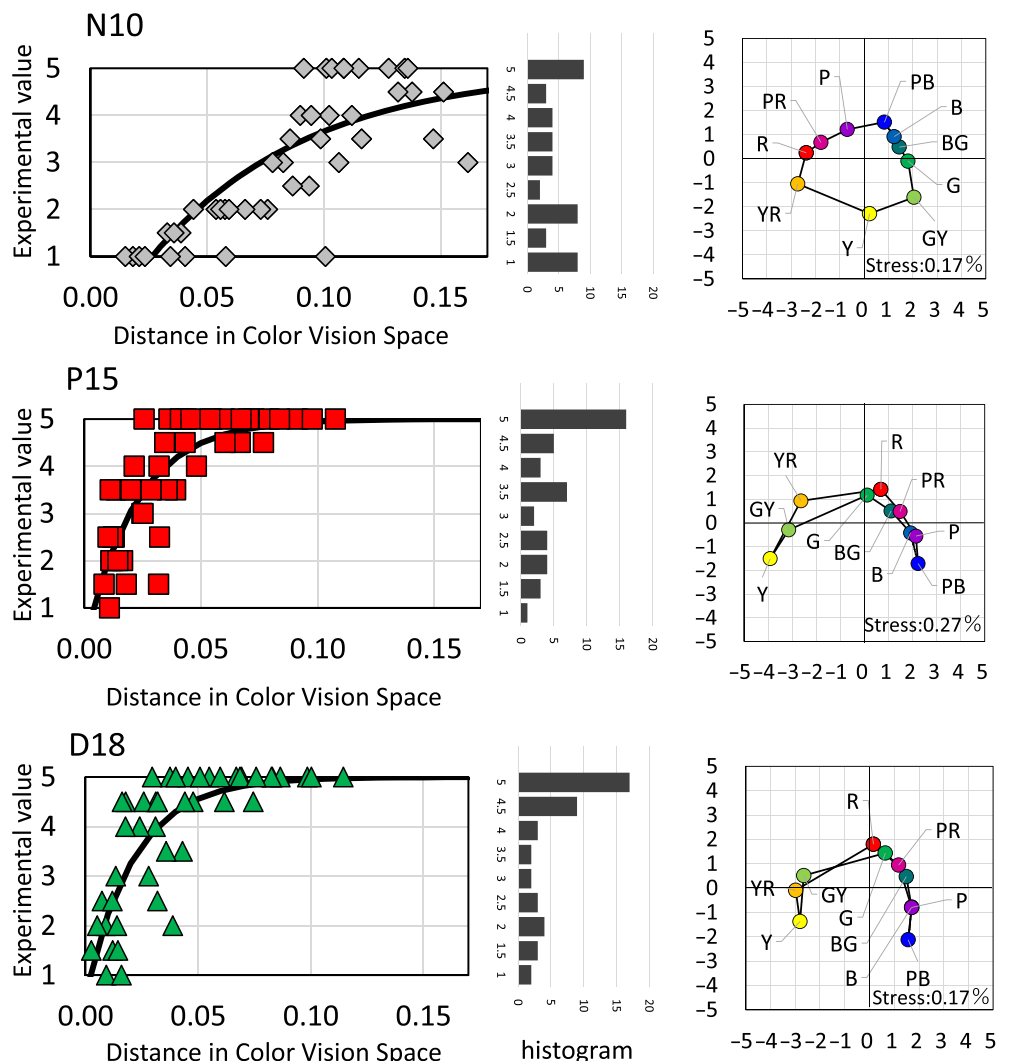


FIGURE 8 Saturation function from the distance in color vision space to the difference scaling scores (left), histogram of the score (center), and the MDS configuration derived from the estimated difference values (right)

a flat ellipsoid, as shown in (vii) in Figure 6. This implies that some kind of transformation is required from the distances in the  $(Ach_k, C_{(r/g),k}, C_{(y/b),k})$  space to the scores of difference scaling, as described in the next section.

#### 4.3 | Transformation from the distance in the $(Ach, C_{(r/g)}, C_{(y/b)})$ space to difference scaling

Examples of the results showing the relation between distance in the  $(Ach_k, C_{(r/g),k}, C_{(y/b),k})$  space and the scores of difference scaling are shown in the left column of Figure 8, as well as in Figure 6(vi). The three graphs in Figure 8 show the results of the same observer, as shown in Figure 4. Points are largely scattered, but the general tendency is that the score increases with the distance in the space for all observers regardless of the color vision type. They do not seem to be fitted by a linear function, and a saturated curve asymptotic to a fixed value appears to be needed. The saturated tendency appears more distinctive in the CDOs' results than in the CNOs. This indicates that the weighted outputs of the luminance, *r/g*, and *y/b* channels in Equations (9)–(11) are not sufficient to describe the results of the difference scaling. In Figure 8, the frequency distribution of the scores is also indicated in the center column. As shown, CDOs tended to assign higher scores (e.g., 4 or 5) more often than CNOs. Based on these findings, we employed a saturation curve expressed in Equation (13) to fit individual results,

$$EV_k = 5 - \alpha_k \cdot 10^{(-\beta_k x)} \quad (13)$$

where  $EV_k$  is the predicted evaluation value of difference scaling,  $x$  is the distance in the  $(Ach_k, C_{(r/g),k}, C_{(y/b),k})$  space, and  $\alpha_k$  and  $\beta_k$  are constants that determine the shape of the curve for observer  $k$ . The constant  $\alpha_k$  should be 5 because it represents the asymptotic value of the equation, and the maximum score employed in the experiment was 5. However, we determined the value of  $\alpha_k$  as a free parameter to obtain the best fit for each observer's result. The constant  $\beta_k$  determines the increase in the curve. As described later, many CDOs have larger  $\beta_k$  values than CNOs.

#### 4.4 | Estimation of individual color representation

There are four constants,  $w_{Lumi}$ ,  $w_{r/g}$ ,  $\alpha$ , and  $\beta$ , to be determined for individual observers. They were determined to

give the best fit in the graph where the difference scaling scores were plotted against the distance in the  $(Ach_k, C_{(r/g),k}, C_{(y/b),k})$  space. In other words, they were determined to minimize the squared sum of the vertical difference between the data point and the predicted curve in the graph shown in the left column of Figure 8. The values of the 45 pairs along the horizontal axis were determined by Equation (12) with  $w_{Lumi,k}$  and  $w_{r/g,k}$ , and those along the vertical axis are determined by Equation (13) with  $\alpha_k$  and  $\beta_k$ , respectively, for observer  $k$ . The best combination of four constants was determined by searching the optimal  $w_{Lumi,k}$  and  $w_{r/g,k}$  combination and  $\alpha_k$  and  $\beta_k$  combination alternately 10 times, confirming the convergence to certain constant values, using the generalized reduced gradient method on linear programming. The solid curves in the left-hand column graphs in Figure 8 indicate the predicted functions for those observers. The values of  $w_{r/g}$ ,  $\alpha$ , and  $\beta$  for individual observers for the results of the high chroma chip are indicated in Table 4. As mentioned before,  $w_{Lumi} = 0$  was obtained for all observers; thus, it is not indicated in Table 4. The correlation coefficient, Pearson's  $R$ , between the predicted  $EV$  values and the experimental rating scores, is indicated in the right-most column. For all observers,  $t$ -value is larger than 5.5 based on 45 pairs and  $p < 0.001$ . The average values of  $R$  for CNOs, protans, and deutans are 0.82, 0.83, and 0.80, respectively, and the grand average of all observers is 0.82, indicating a good performance of the estimation in all three color vision types.

The same calculation was carried out using a linear function between the distance in the  $(Ach_k, C_{(r/g),k}, C_{(y/b),k})$  space and the difference scaling scores for all observers individually. The degree of correlation was worse than those using nonlinear function described above showing the average correlation coefficients for CNOs, protans, and deutans were 0.80, 0.79, and 0.75, respectively. We applied two-way mixed ANOVA with color vision type as between-subject and nonlinear and linear simulation as within-subject factors. Results revealed a main effect of simulation ( $F(1,27) = 39.8$ ,  $p < 0.001$ ,  $\eta^2_G = 0.082$ ) and a main effect of color vision type ( $F(2,27) = 0.718$ ,  $p = 0.497$ ,  $\eta^2_G = 0.048$ ), indicating that the introduction of nonlinearity is effective to improve the data fitting. Examining the pair-comparisons among the groups, the linear versus nonlinear for normal, protan, and deutan were ( $t = 1.726$ ,  $p = 1.000$ ), ( $t = 4.092$ ,  $p = 0.005$ ), and ( $t = 5.113$ ,  $p < 0.001$ ), respectively. This indicates that this nonlinear transformation is particularly effective for the cases of CDOs.

The predicted  $EV$  values for the 45 pairs using Equation (13) were used for MDS analysis. The MDS configurations for observers N10, P15, and D18 derived from the estimated values of difference score using our simulation

**TABLE 4** Parameters indicating individual differences of color space and correlation coefficient between experimental and estimated values of difference scale

Observer		Experiment		Simulation				Correlation coefficient		
		No	Type	Relative distance between R and G (%)	Estimated wavelength separation $\Delta\lambda$	Weighting coefficients of luminance, r/g, and y/b ( $W_{Lumi} = 0$ for all obs.)				
						$W_{r/g}$	$W_{y/b}$	$\alpha$	$\beta$	R
N10	N	93.1		18.5	4.40	1		5.92	6.45	0.806
N11	N	72.8		14.5	4.63	1		4.85	5.53	0.777
N12	N	84.8		16.8	3.70	1		5.87	7.45	0.860
N13	N	86.1		17.1	3.72	1		5.42	6.45	0.791
N14	N	65.2		12.9	3.29	1		5.20	8.30	0.879
N15	N	92.1		18.3	3.01	1		5.86	7.29	0.836
N16	N	86.9		17.3	6.47	1		5.34	4.76	0.758
N17	N	96.0		19.1	4.03	1		5.75	7.12	0.828
N20	N	81.3		16.2	6.24	1		4.79	4.72	0.773
N32	N	93.7		18.6	3.80	1		5.39	7.40	0.866
P3	PA	42.2		8.2	0.55	1		4.62	11.86	0.856
P4	PA	20.8		4.0	1.38	1		4.64	7.95	0.839
P5	P	21.7		4.2	1.47	1		6.01	14.28	0.852
P7	PA	61.5		12.0	2.13	1		4.90	7.25	0.778
P8	PA	95.9		19.0	3.22	1		5.86	7.83	0.849
P9	PA	26.4		5.1	1.05	1		4.47	11.33	0.845
P10	P	52.1		10.2	1.31	1		5.68	21.11	0.776
P11	P	11.3		2.2	1.40	1		5.08	18.59	0.851
P14	P	15.1		2.9	1.54	1		4.88	23.74	0.833
P15	P	22.4		4.3	1.05	1		4.72	19.32	0.822
D7	D	32.9		6.7	0.18	1		4.08	12.85	0.844
D8	D	8.8		1.8	0.00	1		3.71	7.65	0.883
D9	D	41.5		8.4	0.00	1		2.45	26.84	0.683
D10	DA	89.7		17.9	3.36	1		4.64	6.83	0.725
D11	D	39.9		8.1	1.45	1		3.44	7.41	0.644
D12	DA	20.3		4.1	0.69	1		4.53	9.78	0.944
D13	D	96.4		19.2	1.46	1		4.44	5.94	0.801
D14	D	10.1		2.1	0.00	1		3.97	15.34	0.848
D17	D	10.9		2.2	0.70	1		5.26	19.61	0.867
D18	D	7.9		1.6	0.55	1		4.37	19.93	0.805

Note: The colors of Obs. in the table are protanopes for dark orange, protanomalous trichromats for pale orange, deuternopes for dark green, and deuteronomalous trichromats for pale green.

are indicated in the right column of Figure 8. The circular shape of N10 and the concave C-shape of P15 and D18 are predicted by the estimations that are comparable with those of the experimental results shown in Figure 4.

A good correlation between the experimental rating scores and the predicted  $EV$  values was obtained in the medium chroma condition for all observers employing

exactly the same calculation process as in the high chroma condition, introducing a nonlinear transformation at the final stage. The average values of  $R$  between the experimental rating scores and the predicted  $EV$  values for CNO, protans, and deutans in the medium chroma condition were 0.87, 0.92, and 0.93, respectively, and the grand average was 0.90, which was the same

level of good performance as that in the high chroma condition. Seven out of nine protans and four of seven deutans showed non-zero  $w_{\text{Lumi},k}$  indicating luminance difference between the color chips slightly contributes to the difference scaling in the medium-chroma condition while no contribution in the high chroma condition. In the case of CNOs,  $w_{\text{Lumi}} = 0$  for all observers as same as the high chroma condition.

## 5 | DISCUSSION

The color representations of CNOs, protans, and deutans can now be explained successfully using a single model. One reason for obtaining a good fit is that the model considers various levels of human color vision mechanism from the cone pigment absorption to the luminance and opponent-color coding level, and put individual variation parameters according to accumulated knowledge of physiology and psychophysics hitherto reported. It should also be noted that the inclusion of the saturation function from the distance in the individual ( $Ach$ ,  $C_{(r/g)}$ ,  $C_{(y/b)}$ ) space to the difference scaling was substantial to reproduce a well-fitted concave shape. However, the fitting is not perfect. Several reasons can be considered: one is that we did not measure physiological factors for our observers, such as cone pigment genetics, macular pigment and ocular absorbing characteristics, or psycho-physical factors of spectral luminance sensitivity or opponent-chromatic responses. If some of these data were available, we could obtain a better fit.

Compared with the results of previous studies mentioned in Section 1.2, shorter distance between reddish and greenish stimuli relative to that between yellowish and bluish stimuli (e.g., distance between 600 nm, 613 nm and 525 nm, 554 nm relative to that between 570 nm, 575 nm and 466 nm in Paramei,<sup>11</sup> or distance between red and green relative to that between yellow and blue in Lillo et al.<sup>13</sup>) is a common characteristic between their MDS results and ours. However, the MDS configuration in those studies as well as those indicated in Paramei et al.<sup>14</sup> and Bonnardel<sup>12</sup> are rather complicated. Probably because the whiteness judgment or white stimulus was employed<sup>11,13,14</sup> which made the shape of MDS configuration on the first versus second axes plane slightly tangled, or the MDS configuration based on the compromise between color sorting and color naming tasks.<sup>12</sup> General tendencies of the MDS configuration for CNOs and both types of CDOs in this study are the closest to the results of Shepard and Cooper<sup>10</sup> in which they used nine chromatic stimuli covering a hue circle similar to ours. New features indicated in this study not shown in theirs are slight difference between protans and

deutans, the flatter C-shape in medium chroma card unique to protans, the range of individual variability among 10 observers, and the estimation of vision-based color representation based on color vision mechanism.

We understand that our study has certain limitations. Number of observers were 10 for each of CNOs, protans, and deutans, and they were all Japanese males. Also, majority of our CDOs has severe color deficiency, showing wide range in the anomaloscope test. So, the distribution of  $DI$  in Table 3 does not reflect general tendency of each of color vision types but limited to the observers in this study. It is noting that there are overlaps between CNOs and CDOs in  $DI$ ,  $w_{r/g}$ , and  $\beta$  values. To investigate whether those values continuously change from CNOs to CDOs is an interesting issue to be done.

## 6 | CONCLUSION

The results of the difference scaling experiment using 45 pairs from 10 color chips representing basic hues of the Munsell system were analyzed by the MDS to construct the vision-based color representation for CNOs and both types of CDOs, protans and deutans. The vision-based color representation for the CNOs became circular, similar to the Munsell hue circle, whereas those of CDOs showed large individual differences. One protanomalous, one deuteranomalous, and one deutanope observer showed a color representation similar to that of CNOs, while most of the other CDOs showed a concave shape representation bending at Y and PB. A  $DI$  the enclosed area divided by the square of the maximum distance among the 45 pairs, was proposed to express the degree of distortion of the color representation from a circular shape. The  $DI$  of dichromats tended to be larger than that of anomalous trichromats and/or CNOs. This tendency was clearer in the medium chroma results than in the high chroma results.

Next, we first estimated the color representation by estimating the peak wavelength shift of the L or M cone spectral sensitivities based on the shift of the pigment absorbance curve, outputs of 10 color chips, the weighted color vision space of luminance,  $r/g$ , and  $y/b$  channels, and a nonlinear transformation from the distance there to the difference scaling judgment. Good performance was obtained in the estimation of the color representation for CNOs and CDOs for both the high and medium chroma results. The concave shape of the CDOs was successfully predicted by the model.

Using the present model, we can estimate the shape of the color representation of individual observers with five parameters: the wavelength shift of the L and/or M cone spectral sensitivity ( $\Delta\nu$ ), weighting coefficients of luminance and red-green opponent channels ( $w_{\text{Lumi}}$  and

$w_{r/g}$ ), and the parameters to determine the saturation function from the elementary color vision space to the difference rating ( $\alpha$  and  $\beta$ ). Our results showed the validity of the simulation to the extent with a correlation coefficient of 0.82 with the experimental data. Thus, a simplification of the procedure, that is, difference scaling using fewer stimuli, might be able to estimate individual observers color representations, although some verification is necessary.

Currently, personal access devices (PADs) are essential for most people, and their color customization has recently received attention. The most common color modification for CDOs is color enhancement<sup>34</sup>; however, our results imply that individual CDOs require different color enhancements. For one observer, the perceived difference between vivid red and bright green is the same as that between orange and lime green, but for other observers, the difference might be different. Therefore, some procedures are required to optimize color reproduction for PAD users. Difference scaling for several pairs of color stimuli, and some algorithms to enhance display colors according to the user's vision-based color representation would make true color customization possible.

## ACKNOWLEDGMENT

A part of this work was supported by JSPS KAKENHI grant number 15K00278 of which Principal Investigator is S.O. The authors would like to thank Color Universal Design Organization and Kota Kanari to their collaboration to carry out the experiment, and their helpful discussion.

## AUTHOR CONTRIBUTIONS

All authors were involved in the design of the study, discussion of the results, and work on the final manuscripts. M.O. carried out the experiments with support from S.H. M.O., T.I., and M.A developed the simulation model with support from S.H. M.O., T.I., and M.A developed the simulation model project.

## DATA AVAILABILITY STATEMENT

The data that support the findings of this study are available from the corresponding author upon reasonable request.

## ORCID

Minoru Ohkoba  <https://orcid.org/0000-0001-9559-3328>  
Miyoshi Ayama  <https://orcid.org/0000-0001-6562-1367>

## REFERENCES

- [1] Neitz M, Neitz J. Molecular genetics of color vision and color vision defects. *Arch Ophthalmol.* 2000;118(5):691-700. doi: 10.1001/archophth.118.5.691
- [2] Neitz M, Patterson SS, Neitz J. Photopigment genes, cones, and color update: disrupting the splicing code causes a diverse array of vision disorders. *Curr Opin Behav Sci.* 2019;30:60-66. doi:10.1016/j.cobeha.2019.05.004
- [3] Neitz J, Neitz M, Kainz PM. Visual pigment gene structure and the severity of color vision defects. *Science.* 1996; 274(5288):801-804. doi:10.1126/science.274.5288.801
- [4] Pitt FHG. The nature of normal trichromatic and dichromatic vision. *Proc R Soc Lond.* 1944;B132:101-117. doi: 10.1098/rspb.1944.0006
- [5] Paramei GV. Color discrimination across four life decades assessed by the Cambridge colour test. *J Opt Soc Am A.* 2012; 29(2):A290-A297. doi:10.1364/JOSAA.29.00A290
- [6] Rodriguez-Carmona M, O'Neill-Biba M, Barbur JL. Assessing the severity of color vision loss with implications for aviation and other occupational environments. *Aviat Space Environ Med.* 2012;83(1):19-29. doi:10.3357/ASEM.3111.2012
- [7] Shinomori K, Panorgias A, Werner JS. Discrimination thresholds of normal and anomalous trichromats: model of senescent changes in ocular media density on the Cambridge colour test. *J Opt Soc Am A.* 2016;33(3):A65-A76. doi: 10.1364/JOSAA.33.000A65
- [8] Almustanyir A, Hovis J, Glaholt MG. Predicting the Farnsworth-Munsell D15 and Holmes-Wright-a lantern outcomes with computer-based color vision tests. *J Opt Soc Am A.* 2020;37(4):A1-A10. doi:10.1364/JOSAA.381305
- [9] Nakauchi S, Onouchi T. Detection and modification of confusing color combinations for red-green dichromats to achieve a color universal design. *Color Res Appl.* 2008;33(3):203-211. doi: 10.1002/col.20404
- [10] Shepard RN, Cooper LA. Representation of colors in the blind, color-blind, and normally sighted. *Psychol Sci.* 1992;3(2):97-104. doi:10.1111/j.1467-9280.1992.tb00006.x
- [11] Paramei GV. Color space of normally sighted and color-deficient observer reconstructed from color naming. *Psychol Sci.* 1996;7(5):311-317. doi:10.1111/j.1467-9280.1996.tb00380.x
- [12] Bonnardel V. Color naming and categorization in inherited color vision deficiencies. *Vis Neurosci.* 2006;23(3-4):637-643. doi:10.1017/S0952523806233558
- [13] Lillo J, Moreira H, Álvaro L, Davies I. Use of basic color terms by red-green dichromats: 1. General description. *Color Res Appl.* 2014;39(4):360-371. doi:10.1002/col.21803
- [14] Paramei GV, Bimler DL, Cavonius CR. Color-vision variations represented in an individual difference vector chart. *Color Res Appl.* 2000;26(S1):230-234.
- [15] Oliveira MM. Towards more accessible visualizations for color-vision-deficient individuals. *Comput Sci Eng.* 2013;15(5): 80-87. doi:10.1109/MCSE.2013.113
- [16] Waldin N, Bernhard M, Rautek P, Viola I. Personalized 2D color maps. *Comput Graph.* 2016;59:143-150. doi:10.1016/j.cag.2016.06.004
- [17] Okudera S, Sagawa K, Nakajima Y, Ohba N, Ashizawa S. Psychological hue circle of blind people and development of a tactile color tag for clothes. *Proc AIC.* 2015;761-766.
- [18] Sturges J, Whitfield TWA. Locating basic colours in the Munsell space. *Color Res Appl.* 1995;20(6):364-376.
- [19] Berlin B, Kay P. *Basic Color Terms: the Universality and Evolution.* University of California Press; 1969.

- [20] Ayama M, Ohkoba M, Kanari K, Ishikawa T, Hira S, Ohtsuka S. Color representations of red-green color deficient and normal observers using color cards and color names. *Proc. of the 5th Asia Color Association Conference* 2019; 317–322.
- [21] Ayama M, Ohkoba M, Ishikawa T, Hira S, Ohtsuka S. Difference scaling and color naming of red-green color deficiencies. *Proc AIC*. 2021;393–398.
- [22] Jägle H, Pirzer M, Sharpe LT. The Nagel anomaloscope: its calibration and recommendations for diagnosis and research. *Graefes Arch Clin Exp Ophthalmol*. 2005;243:26–32. doi: 10.1007/s00417-004-0893-z
- [23] Kruskal JB. Multidimensional scaling by optimizing goodness of fit to a nonmetric hypothesis. *Psychometrika*. 1964;29:1–27. doi:10.1007/BF02289565
- [24] Hetzner D. Comparing binary image analysis measurements -Euclidean geometry, centroids and corners. *Microscopy Today*. 2008;16(4):10–17. doi:10.1017/S1551929500059721
- [25] Evans B, Rodriguez-Carmona M, Barbur JL. Color vision assessment-1: visual signals that affect the results of the Farnsworth D-15 test. *Color Res Appl*. 2021;46:7–20. doi: 10.1002/col.22596
- [26] Yaguchi H, Luo J, Kato M, Mizokami Y. Computerized simulation of color appearance for anomalous trichromats using the multispectral image. *J Opt Soc Am A*. 2018;35(4):B278–B286. doi:10.1364/JOSAA.35.00B278
- [27] CIE 170-1:2006. *Fundamental Chromaticity Diagram with Physiological Axes-Part 1*. Commission Internationale de l'Eclairage; 2006.
- [28] CIE 170-2:2015. *Fundamental Chromaticity Diagram with Physiological axes-Part 2. Spectral Luminous Efficiency Functions and Chromaticity Diagrams*. Commission Internationale de l'Eclairage; 2015.
- [29] Wyszecki G, Stiles WS. *Color Science: Concepts and Methods, Quantitative Data and Formulae*. 2nd ed. John Wiley & Sons Inc.; 1982:591–604.
- [30] Merbs SL, Nathans J. Absorption spectra of human cone pigments. *Nature*. 1992;356:433–435. doi:10.1038/356433a0
- [31] Merbs SL, Nathans J. Absorption spectra of the hybrid pigments responsible for anomalous color vision. *Science*. 1992; 258(5081):464–466. doi:10.1126/science.1411542
- [32] Deeb SS. The molecular basis of variation in human color vision. *Clin Genet*. 2005;67(5):369–377. doi: 10.1111/j.1399-0004.2004.00343.x
- [33] Hayashi S, Ueyama H, Tanabe S, Yamade S, Kani K. Number and variations of the red and green visual pigment genes in Japanese men with normal color vision. *Jpn J Ophthalmol*. 2001;45(1):60–67. doi:10.1016/S0021-5155(00)00298-7
- [34] CIE 240:2020. *Enhancement of images for colour-deficient observers*. Commission Internationale de l'Eclairage; 2020.

image quality design of the camera system. He is interested in color vision science.

**Tomoharu Ishikawa** obtained a PhD degree from the Japan Advanced Institute of Science and Technology (JAIST) in 2001. He was a post-doctoral student and a research associate for 7 years at JAIST and is currently an associate professor at Utsunomiya University. His recent research interest is KANSEI informatics combining vision, audition, and tactile responses and their application in vividly displaying clothing or food for Internet shopping.

**Shoko Hira** obtained a PhD degree from Kagoshima University, Japan, in 2020. She has been working at the Graduate School of Science and Engineering, Kagoshima University as a technical staff since 2012.

**Sakuichi Ohtsuka** received BS and MS degrees from Kanazawa University, Ishikawa, Japan, in 1978 and 1980, respectively. He received a PhD degree from Hokkaido University, Hokkaido, Japan, in 1990. In 1980, he began working at Nippon Telegraph and Telephone Public Corp (NTT). He moved to Advanced Telecommunications Research Institute International (ATR) in 1993 and returned to NTT in 1996. He moved to NTT DATA Corp in 2001. From 2007 to 2021, he was a Professor at the Graduate School of Science and Engineering, Kagoshima University. Now, he is a Professor in the Department of Science and Technology, International College of Technology, Kanazawa, Japan. His research interests are applied vision, including information display developments, cognitive science, and communication technologies.

**Miyoshi Ayama** obtained a PhD from the Tokyo Institute of Technology (TIT), in Japan, in 1983. After working at Utsunomiya University for 27 years, she is now a Professor Emeritus and a Visiting Professor at the Center for Optical Research and Education at Utsunomiya University, Japan. Her research interest covers various fields in visual science, including basic color vision, color appearance for normal and color deficient observers, glare evaluation of light sources, and lighting effects on the appearance of materials.

## AUTHOR BIOGRAPHIES

**Minoru Ohkoba** is a doctoral student in the Department of Systems Innovation Engineering, Graduate School of Engineering, Utsunomiya University, Japan. He works in a company where he is engaged in the

**How to cite this article:** Ohkoba M, Ishikawa T, Hira S, Ohtsuka S, Ayama M. Color representations of normals and congenital red-green color deficiencies: Estimation of individual results based on color vision model. *Color Res Appl*. 2022;47(3):565–584. doi:10.1002/col.22763